Electronic Supplementary Material (ESI) for ChemComm.
This journal is © The Royal Society of Chemistry 2019

Supporting Information

Two-dimensional (2D) $MnIn_2Se_4$ Nanosheets with Porous Structure: A Novel Photocatalyst for Water Splitting without Sacrificial Agents

Hui Liang,[a] Ting Feng,[a] Shengda Tan,[a] Kaili Zhao,[a] Wei Wang,[a,b] Bohua Dong,*[a] and Lixin Cao*[a]

[a] School of Materials Science and Engineering, Ocean University of China, 238 Songling Road, Qingdao, 266100 P. R. China.

[b] Aramco Research Center Boston, Aramco Services Company, Cambridge, MA02139, USA.

*Corresponding authors' Emails: caolixin@ouc.edu.cn (L. Cao) and dongbohua@ouc.edu.cn (B. Dong)

Experimental Section

Preparation of $MnIn_2Se_4$ Nanosheets: $MnIn_2Se_4$ nanosheets was synthesized by a facile hydrothermal method. Firstly, Indium chloride ($InCl_3$, 0.0591g) and Manganese acetate tetrahydrate ($Mn(CH_3COO)_2,4H_2O$, 0.0319g) were dissolved into 28 mL absolute ethyl alcohol, marked as solution A. 0.0474g selenium powder (Se) was dissolved in 2 ml hydrazine hydrate ($N_2H_4{\cdot}H_2O$), recorded as solution B. Then solution B was slowly dropped into solution A under the continuous stirring. Subsequently, the mixture was transferred to a 50mL Teflon-lined autoclave and maintained at 220℃ for 20 hours. After cooling down to room temperature naturally, the products were collected by centrifugation, then washed three times with deionized water and ethanol, and finally dried in vacuum at 60 °C for 6h in an oven.

Preparation of $CoSeO_3$*2H_2O Nanosheets: 0.249g Cobaltous acetate tetrahydrate ($Co(CH_3COO)_2,4H_2O$) and 0.173g Sodium selenite (Na_2SeO_3) were dissolved in 40 mL mixed solution with a volume ratio of water/diethylenetriamine = 1:2. Afterwards, the mixture was transferred into a 100 mL Teflon-lined autoclave, which was subsequently heated at 180 °C for 16 h. $CoSeO_3$*2H_2O was collected by centrifugation and washed three times with deionized water and ethanol, and dried in oven at 60 °C for 6h.

Preparation of $MnIn_2Se_4$ and $CoSeO_3$*2H_2O Nanosheets: 30mg of as-prepared $MnIn_2Se_4$ nanosheets and a calculated amount of as-prepared $CoSeO_3$*2H_2O (the mass ratio of $CoSeO_3$*2H_2O to $MnIn_2Se_4$ is 1 wt%, 3 wt%, 5 wt%, 10 wt%, 20 wt%) were in a mortar with a small amount of ethanol to grind for 20 minutes. The mixture was subjected to ultrasonication for 2 h and finally dried in oven at 60 °C for 6h.

Characterizations: Crystal phases and structures of the synthesized $MnIn_2Se_4$ and $CoSeO_3$*2H_2O samples were analyzed by power X-ray diffraction (XRD, BRUKER D8 ADVANCE X-ray diffractometer) with Cu Kα radiation from 10° to 80° on increments of 0.019^o, which the scanning speed is 4 °/min. The morphology of the sample were analyzed by transmission electron microscope (TEM, JEOL JEM 1200), scanning electron microscope (SEM, VEGA3 TESCAN) and atomic force microscope (AFM, NT-MDT). Element composition and valence state on the surface of the $MnIn_2Se_4$ was performed on X-ray photoelectron spectroscope (XPS, Kratos Amicus) with an exciting source of Mg and the working power is 180 W. The UV-visible diffuse reflectance absorption spectra of $MnIn_2Se_4$ and $CoSeO_3$*2H_2O samples were analyzed by a UV-vis spectrophotometer (DRS, Solidspec-3700). The Branauer-Emmet-Teller (BET) surface area was measured by nitrogen (N_2) adsorption–desorption at 77 K using a Micromeritics surface area analyzer (ASAP2020) after degassing the samples at 100℃for 24 h. The valance band energy of $MnIn_2Se_4$ nanosheets was tested by Ultraviolet photoelectron spectroscope (UPS, Thermo ESCALAB 250XI). The gas discharge lamp was employed with the admitted helium gas (HeI (21.22 eV) emission line). Photoluminescence spectra (PL) of the

samples were collected at room temperature by a fluorescence spectrometer (Edinburgh FLS980) under the excitation of 400 nm incident light.

Electrochemical Test: Electrochemical measurements were performed on a CHI760E electrochemical workstation (Chenhua Instrument, Shanghai, China) with a conventional three-electrode system cell at room temperature. The working electrode was prepared as following steps: 5 mg of the photocatalyst sample was dispersed in the mixed solution of 300 μL ethyl alcohol and 100 μL acetylacetone, then the mixed solution was subjected to ultrasonication for 10min to form uniform slurry. Finally, the slurry coated onto the surface of the FTO glass electrodes and dried at 60 °C for 2h. The reference and counter electrodes were Ag/AgCl and Pt, respectively. Photoelectric current (I-t) measurements were performed using 300 W xenon lamp as light source and 0.5 M Na_2SO_4 aqueous solution as electrolyte. Electrochemical impedance spectroscope (EIS) measurements were carried out at overpotential of 100 mV with frequency from 0.01 to 100,000 Hz. Mott–Schottky (M–S) analysis were obtained by measuring the spacecharge layer capacitance over a scanned range of applied potentials (-1.5 to 0 V) at 1000 and 800 Hz. The recorded potentials were referenced to NHE according to $E_{(vs\ NHE)} = E_{(vs\ Ag/AgCl)} + E_{(AgCl)}$ ($E_{(AgCl)}$ = 0.197 V).

Photocatalytic Measurement*:* The photocatalytic H_2 evolution experiments were performed in a vitreous reaction cell with a quartz glass cover, which connected to a closed gas circulation system with vacuum and cooling water circulation system at 6℃. Typically, 15 mg photocatalyst sample was dispersed in 100 mL pure water without any sacrifice agent. Subsequently, the reaction was carried out in an aqueous solution in an optical vessel under irradiation of a 300 W Xe lamp. The amount of hydrogen produced was detected and recorded at an hour interval by a gas chromatography (GC7900). The apparent quantum efficiency (AQE) was measured under the same photocatalytic reaction conditions on irradiating by using a 300 W Xe lamp. Photon flux of the incident light was determined using an optical power meter (Model: CEL-NP2000, Beijing China Education Au-Light Co., Ltd). In the AQE test, the reaction mixtures were irradiated for 60 min. AQE was calculated using the following equation:

$$AQE = \frac{2 \times \text{ the number of evolved hydrogen molecules}}{\text{the number of incident photons}} \times 100\%$$

Hydroxyl Radical Detection**:** Electron spin resonance spectrometer was conductd to detect water oxidation intermediate in photocatalytic process. Using 5,5-Dimethyl-1-pyrroline N-oxide (DMPO) as a spin trapping agent to detect hydroxyl radicals. In a typical experiment, the photocatalyst was immersed in 200 μL distilled water and irradiated for 6 min, then 50 μL DMPO was added.Finally, the ESR spectra were collected by Bruker a300 electron spin resonance spectrometer.

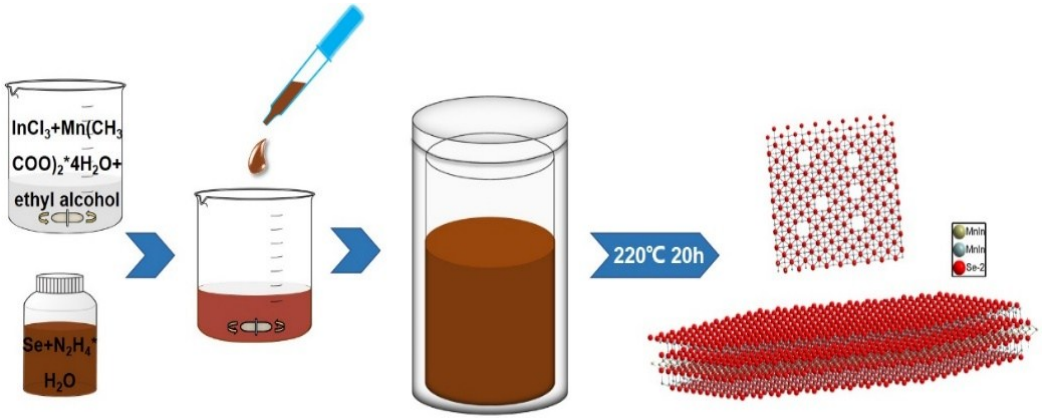

Figure S1. Schematic diagram of synthesis process for $MnIn_2Se_4$.

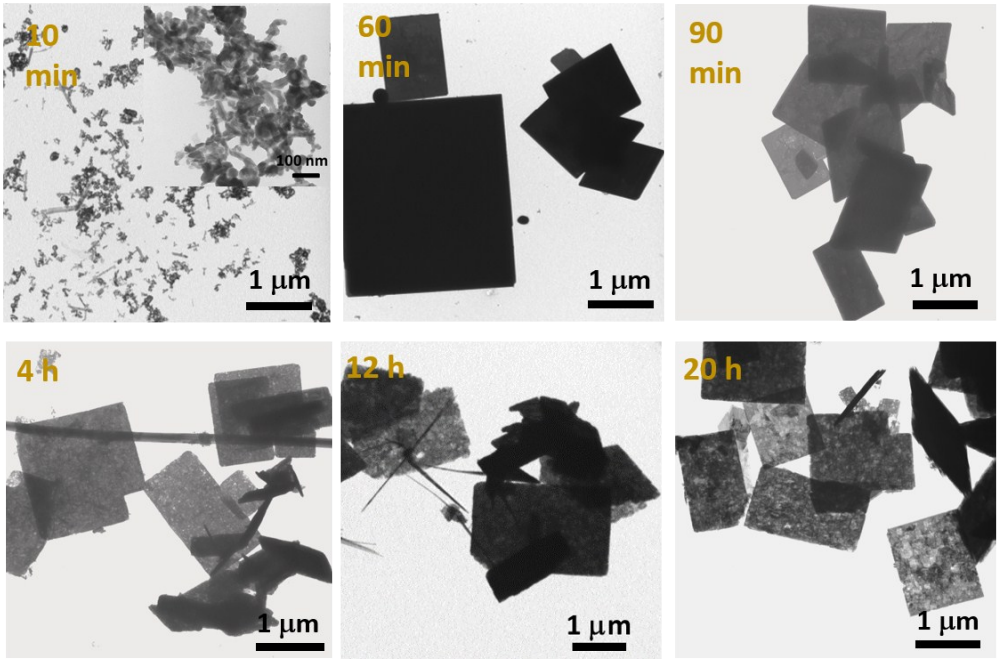

Figure S2. TEM images of $MnIn_2Se_4$ for different reaction time.

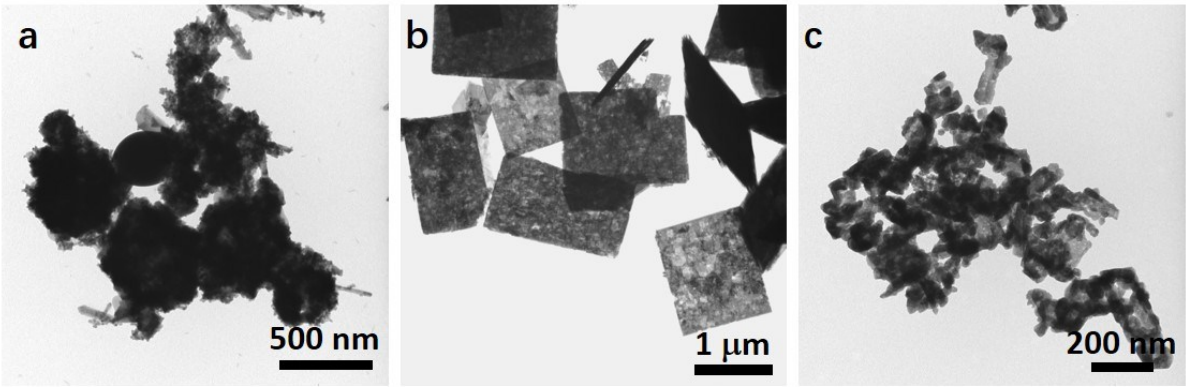

Figure S3. a-c) TEM images of $MnIn_2Se_4$ nanosheets with 0.5ml, 2ml and 4ml hydrazine hydrate added in the synthesis process.

The key factors and formation mechanism for the porous structure should be ascribe to the unique properties of hydrazine hydrate. Hydrazine hydrate is not only a reductant for reducing Se powder, but also a strong alkaline solution, which can corrode $MnIn_2Se_4$ nanosheets to some extent. (*Journal of Colloid and Interface Science 556 (2019) 206–213*) In order to prove the effect of hydrazine hydrate, we supplemented the comparative experiment by adding different volumes of hydrazine hydrate in the synthesis process. As shown in **Figure S3a-c**, the volume of hydrazine hydrate added in the synthesis process is 0.5ml, 2ml and 4ml respectively. When the volume of hydrazine hydrate is 0.5ml, it can be seen that there are obvious black particles, which should be Se powder that has not been completely reduced (**Figure S3a**). When the volume of hydrazine hydrate increased to 4ml, it could be seen that the nanosheet tended to be destroyed (**Figure S3c**). This is due to the excessive hydrazine hydrate which makes the reaction solution more alkaline.

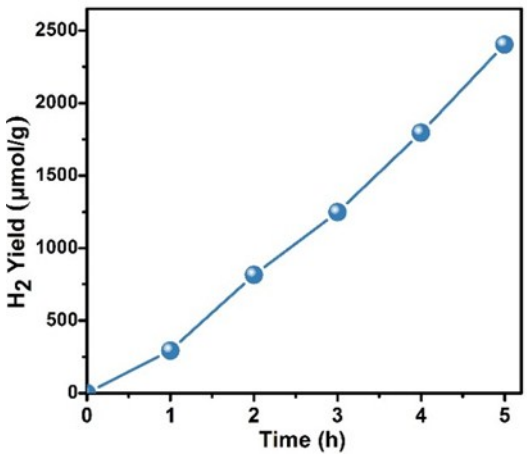

Figure S4. Time course of H_2 evolution performance of $MnIn_2Se_4$. Reaction conditions: 0.015 g of catalyst, 100 mL aqueous solution containing 0.35 M $Na_2S{\cdot}9H_2O$ and 0.25 M Na_2SO_3.

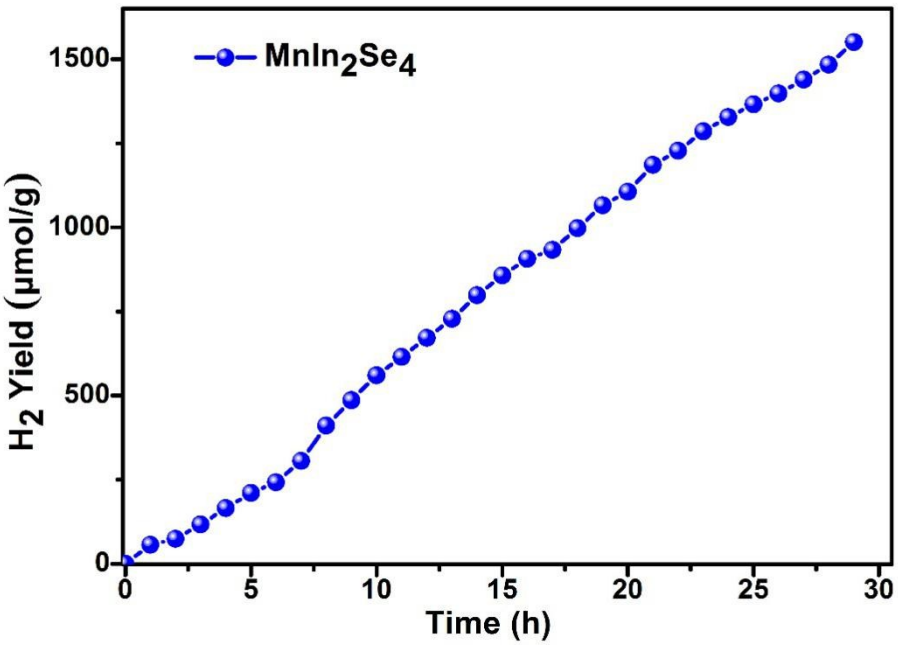

Figure S5. Stability tests of $MnIn_2Se_4$ for photocatalytic H_2 evolution.

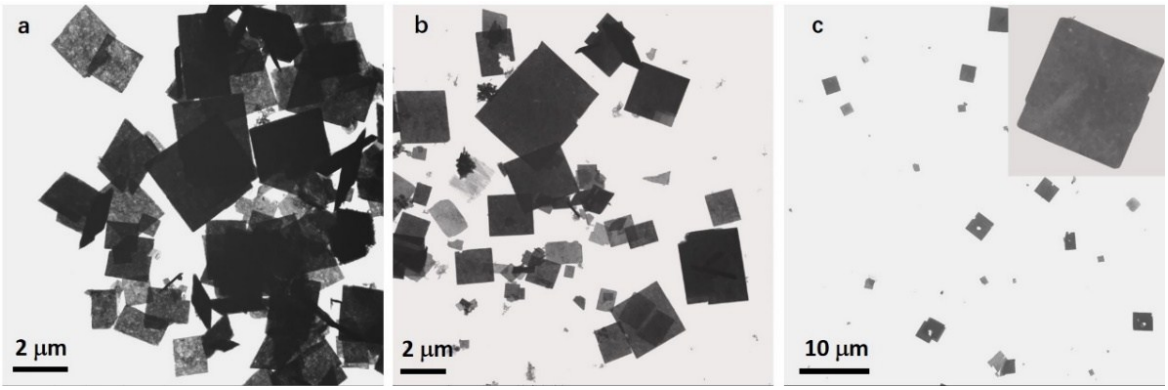

Figure S6. TEM images of $MnIn_2Se_4$ samples was prepared by adding PVP in the process of synthesis: a) 0g PVP; b) 0.2g PVP; c) 0.6g PVP.

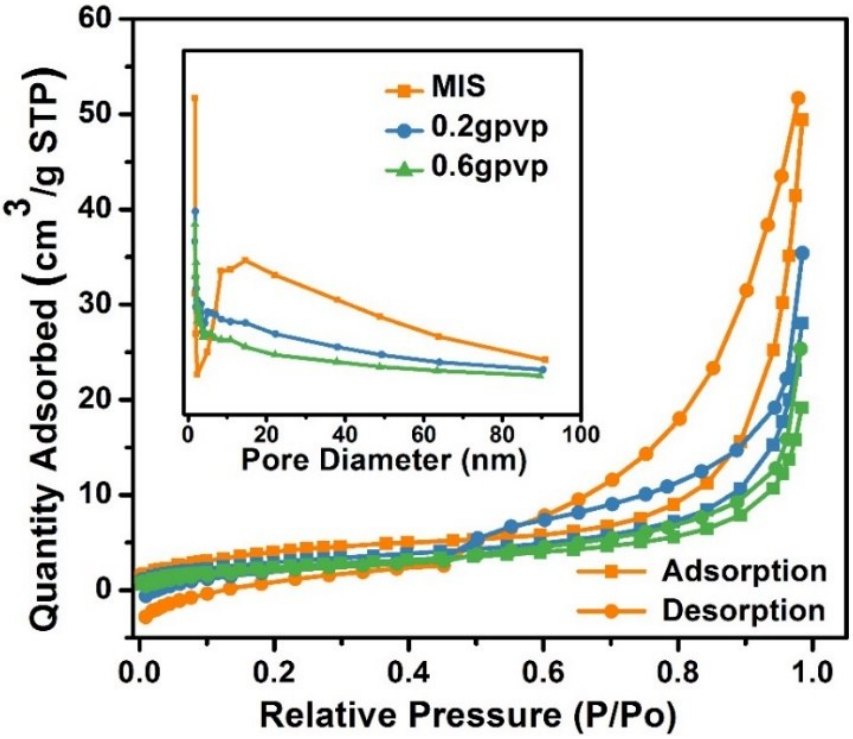

Figure S7. The nitrogen sorption isotherms of as-prepared $MnIn_2Se_4$ with different mass of PVP in the process of synthesis: 0g PVP; 0.2g PVP; 0.6g PVP at 77 K. Inset shows the corresponding BJH pore size distribution curves calculated from the desorption branch.

Table S1. The BET surface area of $MnIn_2Se_4$ and with 0.2g PVP, 0.6g PVP in the process of synthesis, respectively.

Samples	BET Surface Area (m^2/g)
$MnIn_2Se_4$	**15.1345**
$MnIn_2Se_4$ (0.2gPVP)	**11.0453**
$MnIn_2Se_4$ (0.6gPVP)	**9.2979**

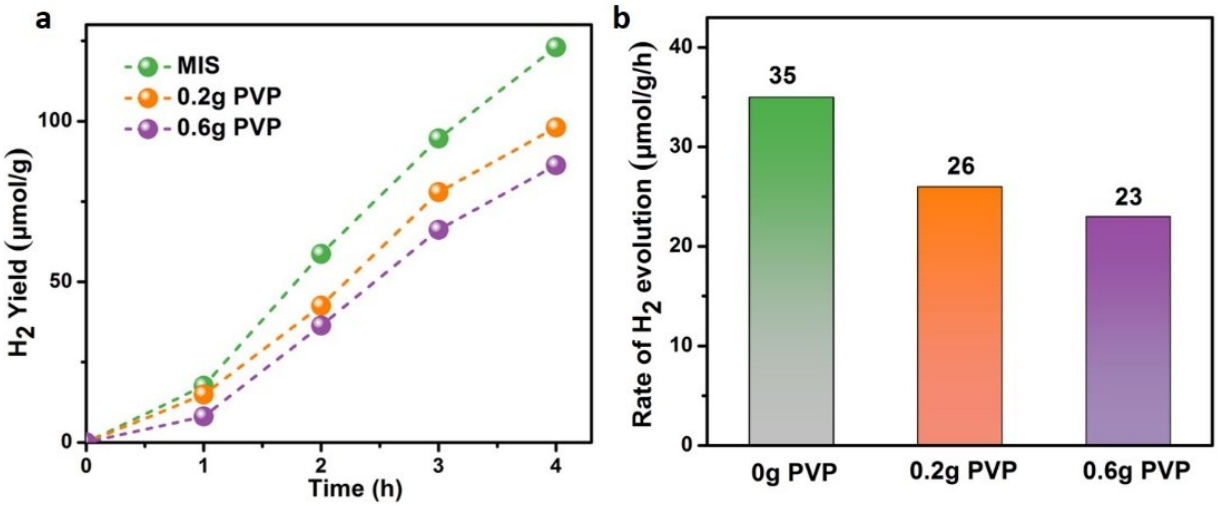

Figure S8. (a) Photocatalytic H_2 evolution of $MnIn_2Se_4$ and with different mass of PVP in the process of synthesis from pure water without any sacrificial agent; (b) the corresponding average hydrogen production rates.

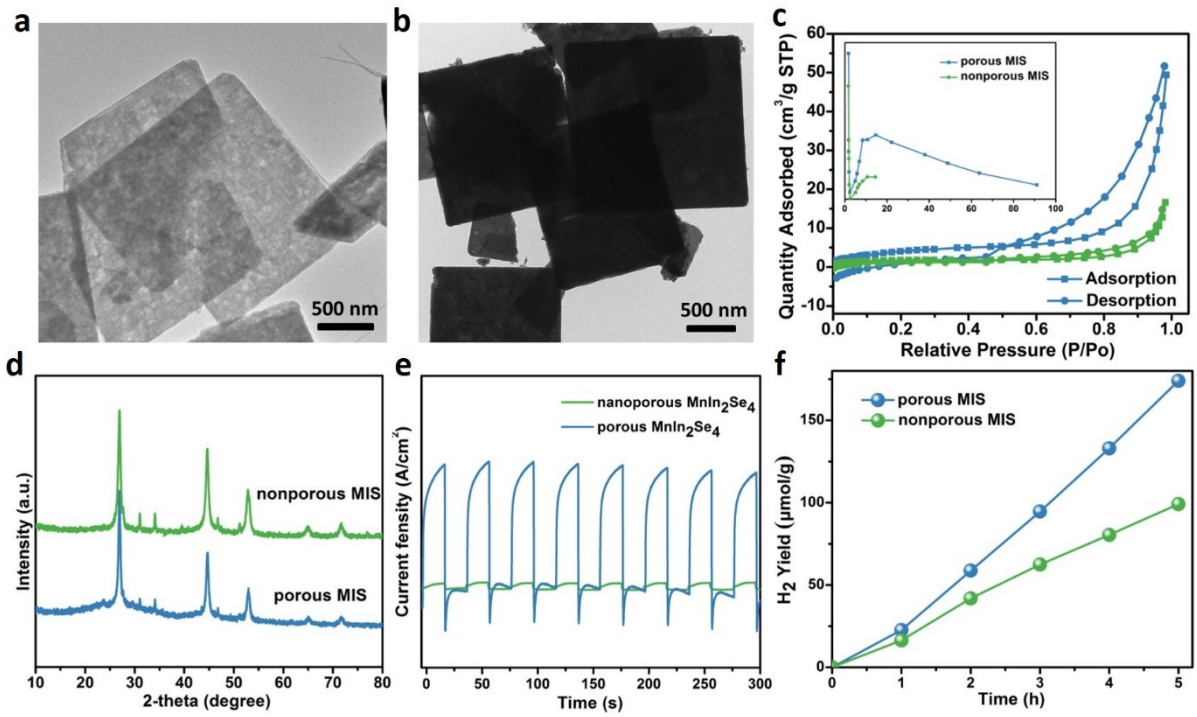

Figure S9. a, b) TEM images of porous and nonporous $MnIn_2Se_4$ nanosheets; c) The nitrogen sorption isotherms of as-prepared porous and nonporous $MnIn_2Se_4$. Inset shows the corresponding BJH pore size distribution curves calculated from the desorption branch. d-f) XRD patterns; transient photocurrent spectra; time course of H_2 evolution performance of porous and nonporous $MnIn_2Se_4$.

The nonporous $MnIn_2Se_4$ nanosheets was synthesized by adding 1.2g polyvinyl pyrrolidone (PVP) in the synthesis process (the sample denoted as $MnIn_2Se_4$-1.2PVP). The TEM images show that porous structure of $MnIn_2Se_4$-1.2PVP samples are relatively unclear than $MnIn_2Se_4$ (**Figure S9a,b**). Furthermore, the results of Brunauer–Emmett–Teller (BET) analysis also confirm it (**Figure S9c**). The BET surface area of porous $MnIn_2Se_4$ is 15.13 m^2/g, which is much bigger than that of nonporous $MnIn_2Se_4$ sample (5.55 m^2/g). Therefore, the sample of $MnIn_2Se_4$-1.2PVP is approximately considered as a nonporous nanosheet. In addition, the comparison between porous and nonporous $MnIn_2Se_4$ were discussed in terms of structure information, carrier transport and photocatalytic activity respectively. As shown in **Figure S9d**, there is no obvious change in the XRD pattern, which indicates that the obtained nonporous $MnIn_2Se_4$ nanosheets retain its pristine crystal structure. To further explore the charge transfer and separation efficiency, the transient photocurrent-time curves of porous and nonporous $MnIn_2Se_4$ samples were measured by several on-off cycles of intermittent

irradiation under visible light (**Figure S9e**). This high photocurrent density further suggesting that porous $MnIn_2Se_4$ had lower recombination rate and a more efficient electron transfer, thus enhancing the photocatalytic hydrogen production activity (**Figure S9f**). This is probably due to the highly porous structure, which gives rise to affluent mass transfer channels and abundant active sites, and shortens the transport distance of carriers. Therefore, based on the experimental results, it can be seen that the porous structure is more favorable for charge carriers transport and separation, which further leads to the improvement of hydrogen evolution efficiency.

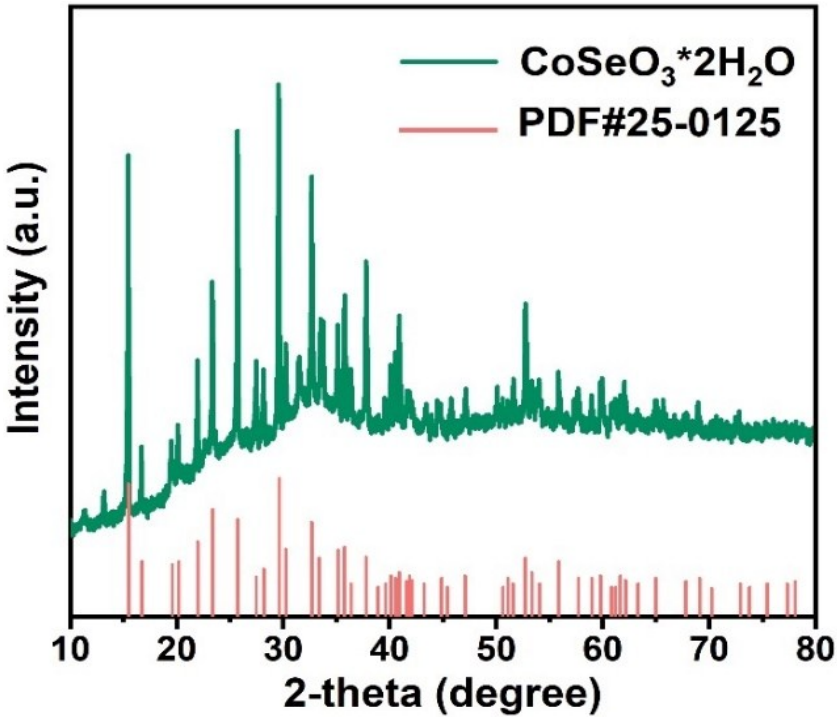

Figure S10. XRD patterns of $CoSeO_3*2H_2O$.

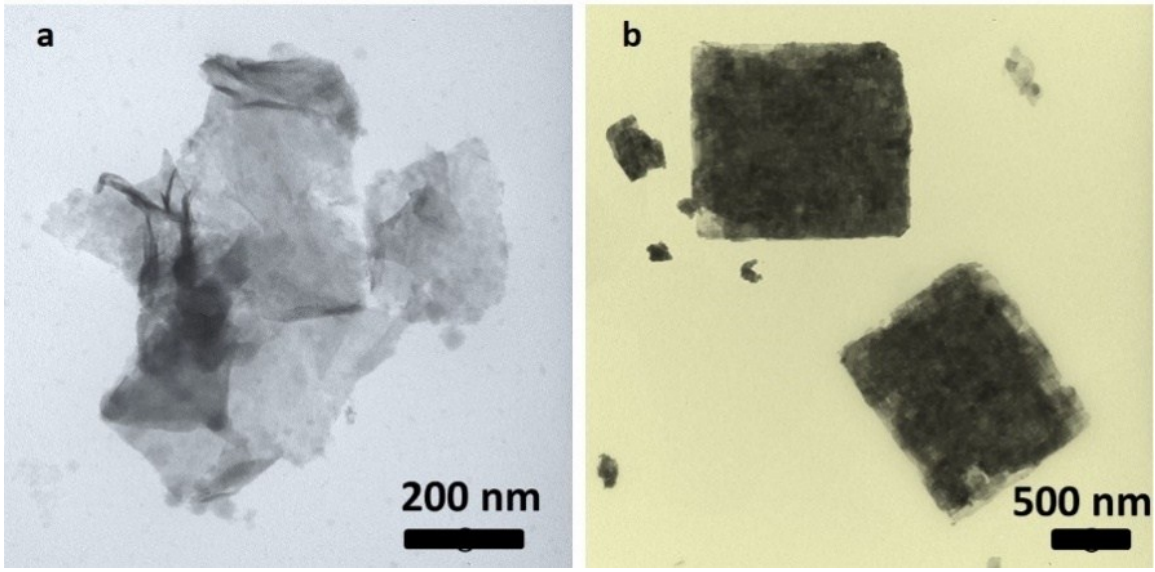

Figure S11. TEM images of (a), $CoSeO_3*2H_2O$ and (b) 5wt% $CoSeO_3$- $MnIn_2Se_4$.

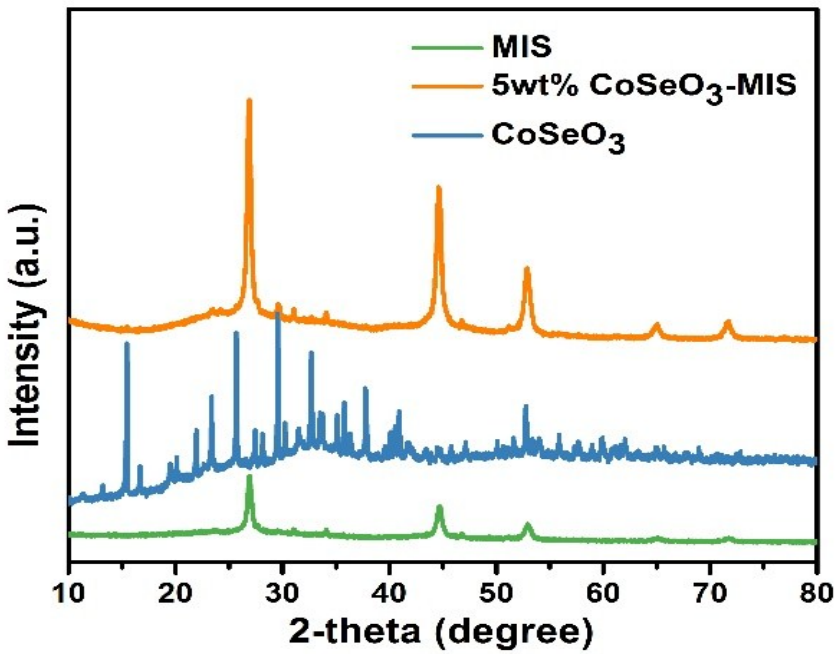

Figure S12. XRD patterns of $CoSeO_3$*$2H_2O$, $MnIn_2Se_4$ and 5wt% $CoSeO_3$- $MnIn_2Se_4$.

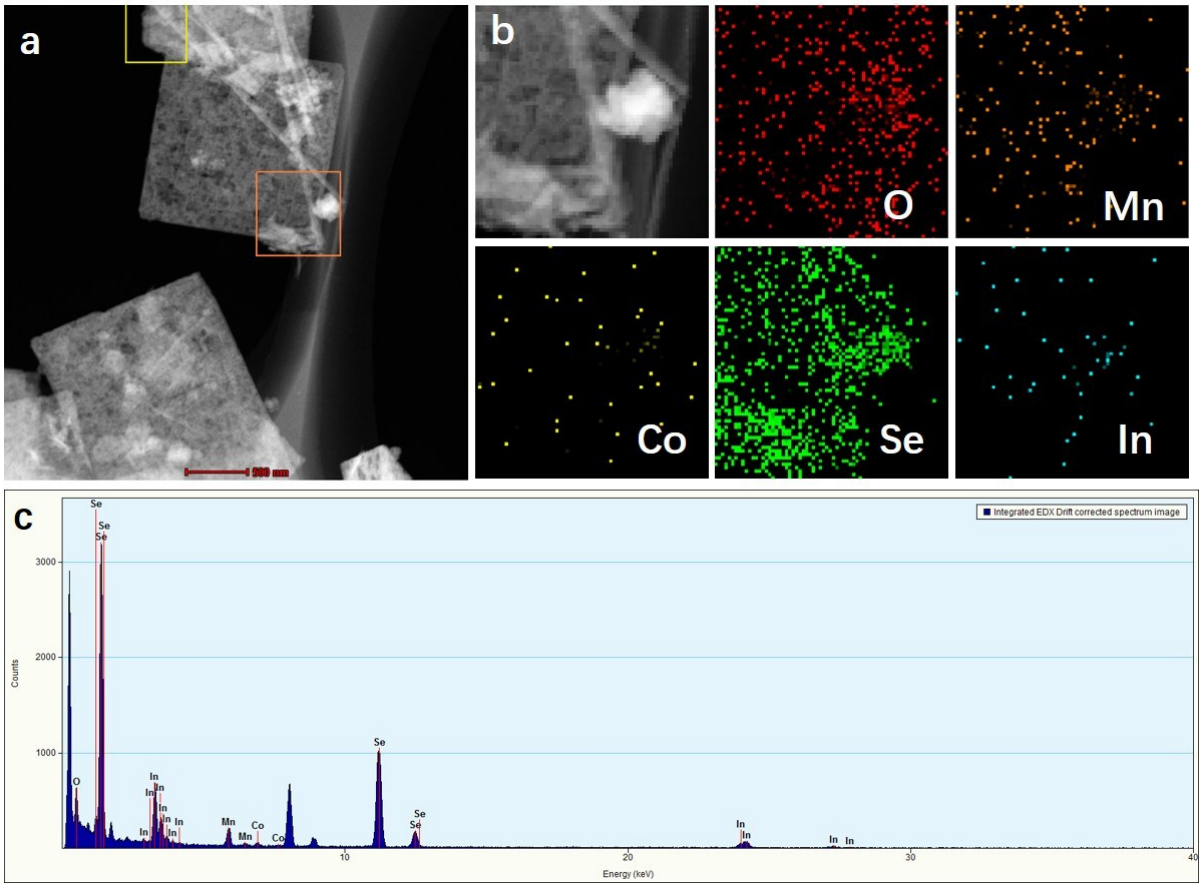

Figure S13. a) STEM, b) elemental mapping images and c) the Energy-dispersive X-ray spectroscopy (EDS) analysis of 5%wt $CoSeO_3$-$MnIn_2Se_4$.

Scanning TEM (STEM) image and corresponding elemental mapping of 5%wt $CoSeO_3$-$MnIn_2Se_4$, as well as the EDS analysis, clearly indicate the existence of Mn, In, Se, O and Co elements in the sample (**Figure S13a-c**).

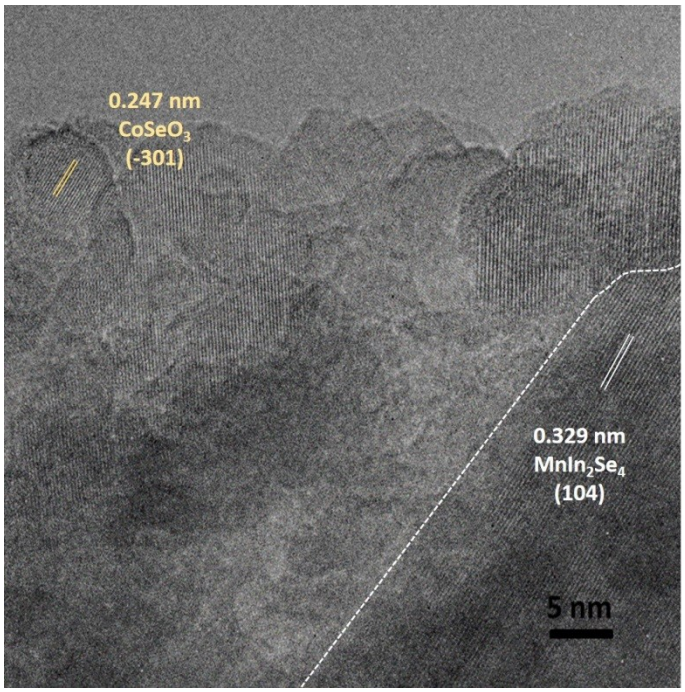

Figure S14. HRTEM image of 5wt% $CoSeO_3$- $MnIn_2Se_4$.

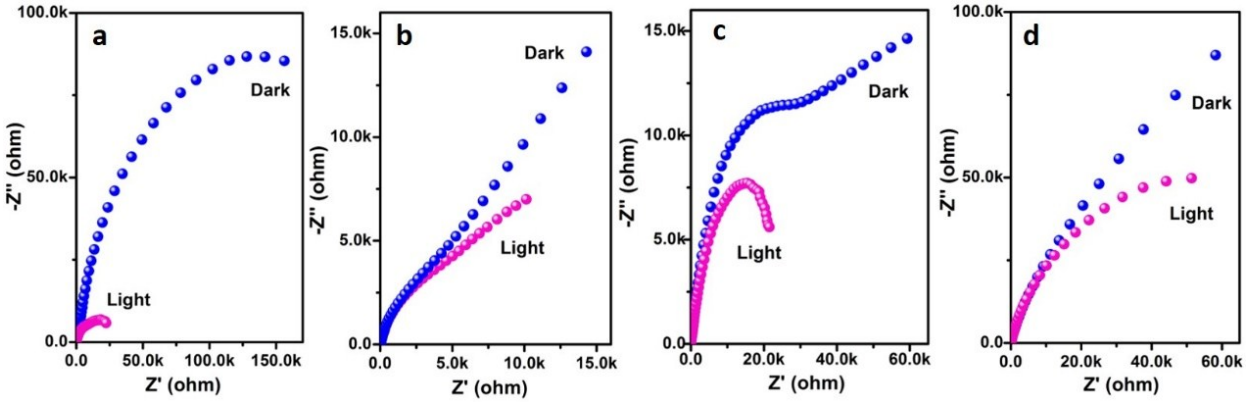

Figure S15. EIS Nyquist plots of different products in dark and light condition: a) $MnIn_2Se_4$; b) 3wt% $CoSeO_3$- $MnIn_2Se_4$; c) 5wt% $CoSeO_3$- $MnIn_2Se_4$ and d) 10wt% $CoSeO_3$- $MnIn_2Se_4$.

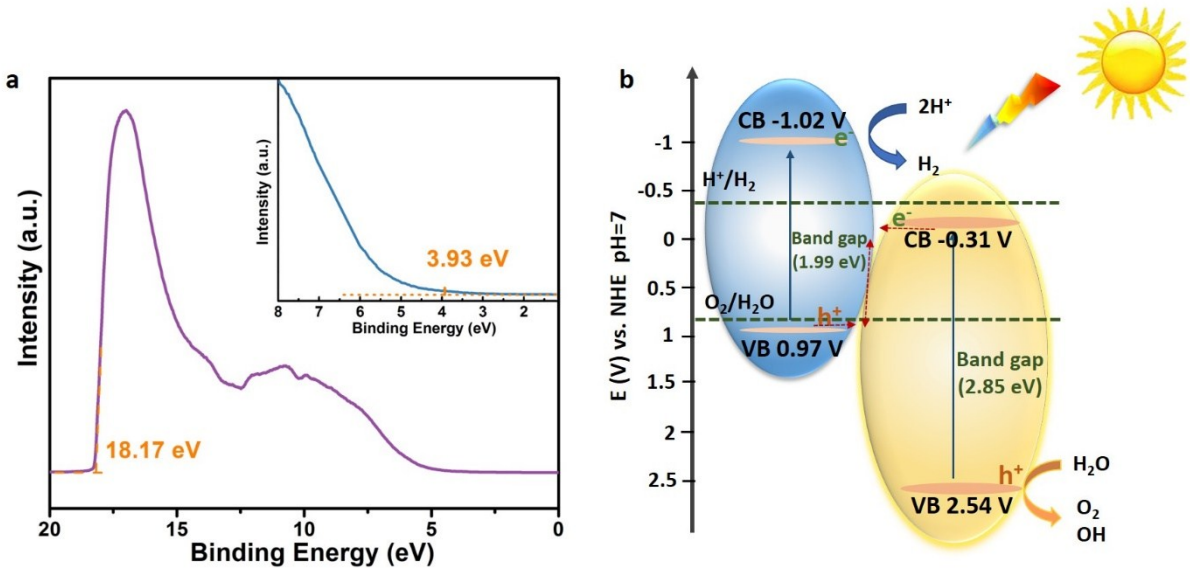

Figure S16. a) Ultraviolet photoelectron spectra of $CoSeO_3$; b) Schematic diagram of the proposed charge carrier transfer and hydrogen evolution mechanism over the $CoSeO_3$-$MnIn_2Se_4$ photocatalyst.

Ultraviolet photoelectron spectroscopy (UPS) is also an effective way to get the absolute position of valance band (VB). We have provided the band positions of $MnIn_2Se_4$ nanosheets by analyzing the results of UPS and Mott–Schottky plots in the manuscript. The VB and conduction band (CB) energy levels of $MnIn_2Se_4$ were observed at 0.97 and 1.02 eV, respectively. Additionally, we also employed UPS get the absolute position of VB of the $CoSeO_3$ sample. By subtracting the width of He I UPS spectra from the system excitation energy of 21.22 eV (**Figure S16a**), one can see that the VB levels of $CoSeO_3$ is at 2.54 versus normal hydrogen electrode (*NHE*) (−6.98 eV vs Vacuum), From the literature, the values band gap energy of $CoSeO_3$ was found to be 2.85 eV. (*Materials Research Bulletin 99 (2018) 161–167*) Therefore, according to the formula $E_{CB} = E_g - E_{VB}$: the CB energy level of $CoSeO_3$ can be calculated as -0.31 versus *NHE*. Based on the information of the band gap energy, we proposed the effective vectorial Z-scheme charge-carrier transfer at the interface of $MnIn_2Se_4$ and $CoSeO_3$ (**Figure S16b**).

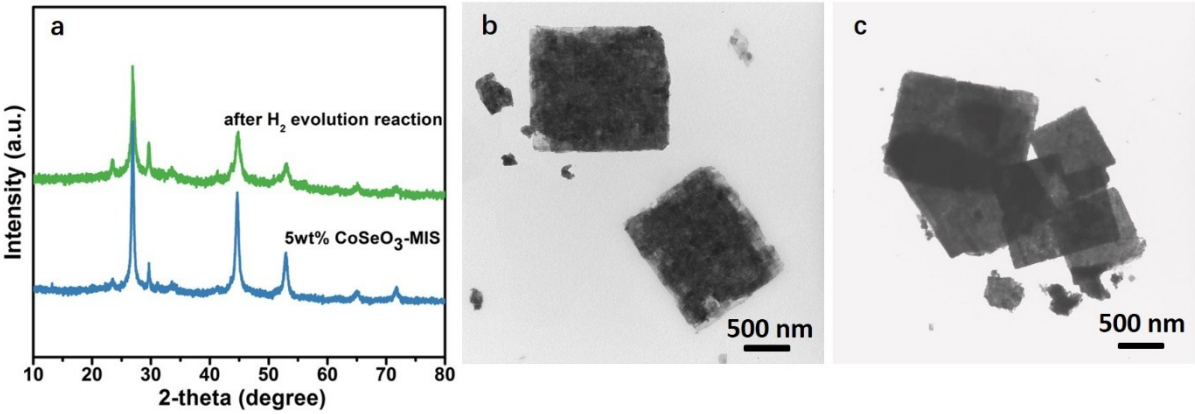

Figure S17. a) XRD patterns of 5%wt$CoSeO_3$- $MnIn_2Se_4$ before and after hydrogen evolution reaction; b)TEM image of 5%wt$CoSeO_3$- $MnIn_2Se_4$ before hydrogen evolution reaction; c) TEM images of 5%wt$CoSeO_3$- $MnIn_2Se_4$ after hydrogen evolution reaction.

This shows the TEM images and XRD pattern for $CoSeO_3$-$MnIn_2Se_4$ after the photocatalytic hydrogen evolution process. There is no change in the TEM images and XRD patterns of the 5%wt $CoSeO_3$-$MnIn_2Se_4$ samples after the hydrogen evolution reaction, which indicates that the photocatalysts are relatively stable in the photocatalytic hydrogen evolution process.